PHYSICAL REVIEW B **85**, 205113 (2012)

Insulator-to-metal transition and correlated metallic state of V_2O_3 investigated by optical spectroscopy

M. K. Stewart,[1,*] D. Brownstead,[1] S. Wang,[2,3] K. G. West,[2] J. G. Ramirez,[2] M. M. Qazilbash,[4] N. B. Perkins,[5]
I. K. Schuller,[2,3] and D. N. Basov[1]
[1]*Department of Physics, University of California–San Diego, La Jolla, California 92093, USA*
[2]*Department of Physics, Center for Advanced Nanoscience, University of California–San Diego, La Jolla, California 92093, USA*
[3]*Materials Science and Engineering Program, University of California–San Diego, La Jolla, California 92093, USA*
[4]*Department of Physics, The College of William and Mary, Williamsburg, Virginia 23185, USA*
[5]*Department of Physics, University of Wisconsin–Madison, Madison, Wisconsin 53706, USA*
(Received 30 December 2011; published 9 May 2012)

The optical properties of V_2O_3 thin films are investigated across the insulator-to-metal transition and in the metallic state. The spectral weight transfer observed across the transition, over an energy scale of 5 eV, is consistent with the Mott-Hubbard model for correlated electron systems. In the metallic phase, a strong Drude peak is observed, which exhibits a pronounced temperature dependence related to the transfer of states from the Hubbard bands to the quasiparticle peaks as the temperature is reduced. The analysis of the far-infrared spectra reveals signatures of strong electronic correlations in V_2O_3. Finally, a comparison to VO_2 data is presented.

DOI: 10.1103/PhysRevB.85.205113 PACS number(s): 78.20.−e, 71.30.+h

I. INTRODUCTION

Many correlated electron systems exhibit phase transitions that can be driven by a variety of external factors and have repercussions that often extend beyond the immediate vicinity of the transition.[1,2] V_2O_3, commonly considered the canonical Mott-Hubbard system, presents a temperature-induced inuslator-to-metal transition (IMT) at $T_c \approx 150$ K. This transition from an antiferromagnetic insulating (AFI) phase to a paramagnetic metal (PM) is accompanied by a change in the crystal symmetry from monoclinic to rhombohedral.[3] The optical properties of V_2O_3 across this IMT and in the correlated metallic state were initially described with the single-band Hubbard model within the framework of dynamical mean-field theory (DMFT).[4,5] While this work represented a breakthrough in the understanding of the Mott-driven IMT, later studies have shown that the multiband character of V_2O_3 must be taken into account.[6,7] The exact configuration of the t_{2g} manifold near the Fermi level, however, is still subject to controversy.[8–13]

In addition to the aforementioned IMT, a high-temperature paramagnetic insulating (PI) phase can be attained in V_2O_3 by applying external pressure and by chemical doping.[14–16] In stoichiometric V_2O_3, a *crossover* region between the PM and PI phases exists at elevated temperatures.[17] Recent x-ray-absorption experiments show variations in the orbital occupation of the metallic state reached through different paths across the phase diagram.[18] These results point to the interplay between electronic correlations and the crystal field as a key factor governing the IMT.

In this work we present an optical study of V_2O_3 thin films showing a significant enhancement of the Drude peak relative to previous samples.[19] The broad energy range and detailed temperature dependence of our data allow us to thoroughly investigate the optical properties both across the AFI to PM transition and above T_c. We report on canonical optical signatures of Mott transitions observed in our data, including evidence of a pseudogap near the IMT. Our results unveil a number of similarities between the properties of the PM state of V_2O_3 and the metallic puddles found in phase separated VO_2.[20,21]

II. METHODS

V_2O_3 thin films were grown by rf magnetron sputtering of a V_2O_3 target (1.5 in. diameter, $>99.7\%$, ACI Alloys, Inc.) on an r plane $(10\bar{1}2)$ sapphire substrate. The sample was prepared in a high vacuum deposition system with a base pressure of 1×10^{-7} Torr. 4 mTorr ultrahigh purity (uhp) Ar was used for sputtering. The substrate temperature during deposition was 750 °C, while the rf magnetron power was kept at 100 W. These conditions yielded a deposition rate of 0.67 Å/s and a total thickness of 100 nm for the sample reported here. The sample was cooled at a rate of 13 °C/min in the same Ar flow after the deposition. Macroscopic resistance vs temperature $(R-T)$ measurements show a metal-insulator transition at 150 K with more than five orders of magnitude change in resistance. Finally, half of the sample was annealed for 30 min. at each 550 and 650 °C with a base pressure of 1×10^{-5} Torr. Most of this paper will focus on the data obtained for the pristine sample. Results for the annealed film are shown in Sec. III E.

Optical characterization of the V_2O_3 film and the sapphire substrate was carried out using spectroscopic ellipsometry in the range from 70 meV to 6 eV and near normal incidence reflectance in the range from 6 to 85 meV. Ellipsometric measurements were performed in two commercial Woollam ellipsometers equipped with home-built UHV cryogenic chambers to allow for low-temperature studies. The optical conductivity of the film was obtained from the raw reflectance and ellipsometry data using a two-layer model taking into account the reflections from the film/substrate interface and the temperature dependence of the substrate. A detailed description of experimental and analysis methods can be found in Refs. 22 and 23.

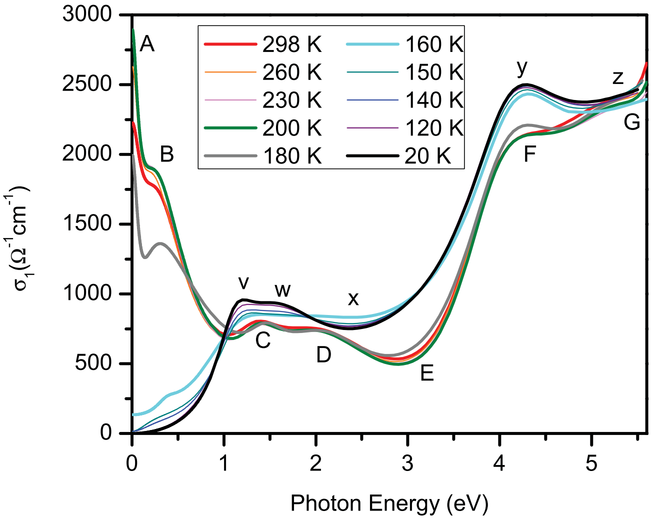

FIG. 1. (Color online) Real part of the optical conductivity of pristine V_2O_3 across the insulator-to-metal transition. Interband transitions in the insulating state are labeled v–z. A–G correspond to features in the metallic phase. See text and Fig. 2 for details.

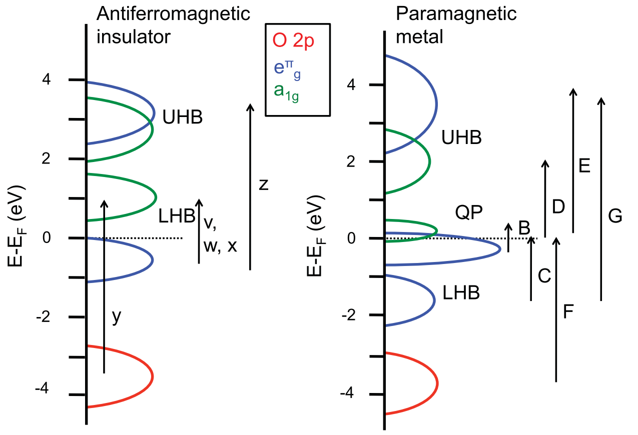

FIG. 2. (Color online) Sketch of the electronic density of states for the antiferromagnetic insulator (Ref. 25) (left) and the paramagnetic metal (Ref. 26) (right) phases of V_2O_3. The assignment of interband transitions corresponds to the labeling of the optical conductivity features shown in Fig. 1.

III. RESULTS AND DISCUSSION

A. Optical conductivity: General trends

We begin by considering the real, dissipative part of the optical conductivity $\sigma_1(\omega)$, which is related to the complex dielectric function through the equation $\sigma(\omega) = \frac{i\omega[1-\epsilon(\omega)]}{4\pi}$. The low-temperature spectra in Fig. 1 show the sample in the insulating state, where $\sigma_1(\omega)$ exhibits an energy gap of $\sim$0.5 eV and a number of interband transitions above 1 eV. As the temperature increases the gap is gradually filled with states and a Drude mode emerges above 180 K along with a finite energy peak centered at 0.27 eV. Additionally, the spectral weight associated with the interband transitions above 1 eV is reduced relative to the insulating state. In comparison to earlier optical data for V_2O_3 thin films,[19] two important differences are evident: (i) The optical conductivity due to interband transitions (above 1 eV) is higher in the insulating state than in the metallic state. This is in contrast with the data in Ref. 19 where the low- and high-temperature $\sigma_1(\omega)$ curves cross at 3 eV. (ii) The Drude peak is much stronger than the weak mode observed previously and is in fact of similar magnitude to that observed in single-crystal samples of V_2O_3.[24] In contrast with Ref. 24, in this work we focus our attention on the antiferromagnetic insulator to paramagnetic metal transition and we examine a much wider energy range of the optical conductivity, up to 6 eV. Below we discuss the spectra in Fig. 1 in relation to theoretical results and earlier measurements on V_2O_3 and VO_2.

We focus first on the optical conductivity at 20 K, corresponding to the insulating state. The left panel in Fig. 2 shows a sketch of the density of states for the antiferromagnetic insulating state based on the LDA + U calculations shown in Ref. 25. The vanadium t_{2g} orbitals are occupied by two electrons and split into nondegenerate a_{1g} (green) and doubly degenerate e^{π}_g (blue) bands due to the trigonal field. Additionally, the strong on-site Coulomb repulsion ($U = 4.2$ eV in Ref. 26) splits each t_{2g} level into upper and lower Hubbard bands (UHB and LHB, respectively). The oxygen $2p$ bands are located about 4 eV below the Fermi level and lower.[19] Based on this picture, we assign features v–z to interband transitions, as depicted in Fig. 2. Peaks v, w, and x are due to transitions within the lower Hubbard bands of the t_{2g} manifold. Features y and z are due to excitations from the O $2p$ bands to the LHB and from the LHB to the UHB, respectively. We note that the work in Ref. 25 results in a ground state in which the a_{1g} LHB is not occupied. This is in contrast with x-ray-absorption studies revealing an AFI ground state with an $(e^{\pi}_g e^{\pi}_g)$:$(e^{\pi}_g a_{1g})$ occupation ratio of 2:1.[6] For this reason, transitions within the LHB result in a series of peaks between 1 and 3 eV rather than the single structure one might expect from the simplified picture in Fig. 2.

In considering the spectra for the metallic state between 200 and 298 K, we refer the LDA + DMFT predictions from Ref. 26. In addition to the LHB and UHB present at low temperature, two quasiparticle peaks (QP) emerge at the Fermi level (see right panel in Fig. 2). The a_{1g} orbitals are nearly empty and have coherent character at the Fermi level, giving rise to the narrow Drude mode (A in Fig. 1). Some e^{π}_g contribution to the Drude peak is also possible, as these bands are expected to approach the regime of coherent quasiparticles below 390 K.[26] Feature B can be assigned to transitions from the e^{π}_g QP to the a_{1g} QP. C and D are due to transitions from the e^{π}_g LHB to the QP and from the QP to the a_{1g} Hubbard band, respectively. Features F and G correspond to transitions within the e^{π}_g bands, from the QP to the UHB and between the lower and upper Hubbard bands. Finally, peak E is related to transitions from the oxygen $2p$ bands. These assignments are, in general, consistent with those in previous optical studies.[19,24] However, here we compare our data to DMFT results taking into account the strongly correlated nature of the metallic phase, i.e., the presence of the Hubbard bands and quasiparticle peaks. The high quality of our films and the detailed temperature dependence of our data allow for more specific assignments and depth of analysis. In the following section we examine features A–G in the context of the Mott-Hubbard model.

B. Metallic state of V_2O_3

To better understand the properties of the metallic state of V_2O_3 we study the temperature dependence between 200 and 298 K. It is useful to consider two quantities: the Drude plasma frequency ω_p and the effective spectral weight as a function of frequency SW(ω), given by

$$\frac{\omega_p^2}{8} = \int_0^{\Omega} \sigma_1(\omega)d\omega = \frac{4\pi n e^2}{m^*}, \tag{1}$$

$$\mathrm{SW}(\omega) = \int_0^{\omega} \sigma_1(\omega')d\omega'. \tag{2}$$

The former is related to the free-carrier density n and effective mass m^*, while the latter represents the effective number of carriers contributing to absorption below the frequency ω. In the case of ω_p, the integration cutoff is chosen such that only the Drude contribution to the optical conductivity is included, leaving out the spectral weight due to interband transitions. The inset in Fig. 3(a) shows ω_p obtained using $\Omega = 140$ meV, before the onset of feature A. An increase from 1.14 eV at 298 K to 1.25 eV at 200 K is evident, signifying an enhancement in the free-carrier density (the temperature dependence of m^* is discussed at the end of this section). Furthermore, in Fig. 3(a) the ratio of SW(ω) at 200 and 298 K shows that, within the metallic state, the low-temperature SW(ω) remains higher up to 3.5 eV. This means that interband transitions up to 3.5 eV must be taken into account in order to explain the low-temperature increase in the Drude SW, as is often the case in correlated metals.[22,23] Looking at the difference between the $\sigma_1(\omega)$ spectra at 200 and 298 K [Fig. 3(b)], it is evident that a transfer of SW from features C, D, and E to features A and B is taking place.

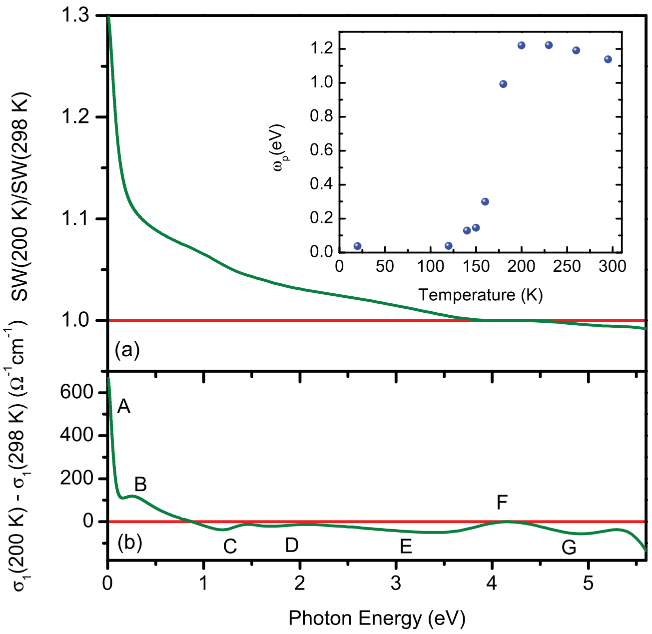

FIG. 3. (Color online) Ratio of the spectral weight at 200 and 298 K (a). Inset: Drude plasma frequency obtained from Eq. (1) with the integration cutoff 140 meV. Difference between the optical conductivity spectra at 200 and 298 K (b). Intra- and interband transitions are labeled as in Fig. 1.

The study of the temperature dependence described above confirms the assignments of features A–G (Fig. 2) in the context of the DMFT predictions for Mott-Hubbard systems.[5,26] At low temperatures, a transfer of SW from the Hubbard bands to the quasiparticle peak is expected. This is evidenced in our data by the increase in SW of the features associated with the QP (A and B) at the expense of those related to the Hubbard bands (C–E). The optical conductivity of feature G is also reduced at 200 K, consistent with the assignment of this peak to transitions between the LHB and the UHB.

We note that the ω_p values reported in the inset of Fig. 3 are low compared to the band theory prediction, giving a ratio $K_{\mathrm{exp}}/K_{\mathrm{band}} = 0.12$ at 200 K. Here K_{exp} and K_{band} represent the electronic kinetic energy obtained from experiment and from band theory, respectively, and their ratio is used to quantify the strength of electronic correlations.[27] K_{exp} is extracted from the optical conductivity using

$$K_{\mathrm{exp}} = \frac{\hbar a}{e^2}\int_0^{\Omega} \frac{2\hbar}{\pi}\sigma_1(\omega)d\omega, \tag{3}$$

where $a = 3$ Å is the lattice constant and Ω is the same as in Eq. (1). While this value represents a factor of 2 increase from the previous generation of V_2O_3 films, it is still very much in the strongly correlated regime lying between the nickelates ($K_{\mathrm{exp}}/K_{\mathrm{LDA}} \approx 0.04$–$0.1$)[22,23,28] and the cuprates ($K_{\mathrm{exp}}/K_{\mathrm{LDA}} \approx 0.15$–$0.45$).[27,29]

In addition to the spectral weight, important information about the metallic behavior of V_2O_3 can be obtained from the extended Drude analysis. This theory is often used in the study of correlated metals as it allows for the frequency dependence of the carrier scattering rate

$$\frac{1}{\tau(\omega)} = \frac{\omega_p^2}{4\pi}\frac{\sigma_1(\omega)}{\sigma_1^2(\omega)+\sigma_2^2(\omega)}, \tag{4}$$

which cannot be assumed to be a constant as in the case of conventional metals.[2] Additionally, the effective mass of the carriers m^*, which in the presence of correlations often shows a strong frequency dependence and an enhancement relative to the band mass m_b, can be obtained from

$$\frac{m^*(\omega)}{m_b} = \frac{\omega_p^2}{4\pi\omega}\frac{\sigma_2(\omega)}{\sigma_1^2(\omega)+\sigma_2^2(\omega)}. \tag{5}$$

The inset in Fig. 4(b) shows $1/\tau(\omega)$ at various temperatures plotted with the gray line representing $1/\tau(\omega) = \omega$. It is evident that $1/\tau(\omega) > \omega$ up to 0.4 eV, in violation of the canonical criterion for well-defined quasiparticles: $1/\tau(\omega) \ll \omega$. Thus, the charge carriers in V_2O_3 are not well-defined quasiparticles and cannot be described by Fermi-liquid theory. Another important aspect of the $1/\tau(\omega)$ spectra seen in Fig. 4(b) is the maximum appearing at 200 K centered around 0.18 eV. This type of structure in the scattering rate has been observed in other correlated oxides such as the high-T_c cuprates, nickelates, and VO_2,[21] oftentimes in the vicinity of an IMT. It can be attributed to the presence of a pseudogap: a partial gapping of the Fermi surface leading to a suppression in the scattering rate at low frequencies. The mass enhancement factor [Fig. 4(c)] exhibits a strong frequency dependence, particularly at low temperatures. Additionally, in the low-frequency limit m^*/m_b increases as the temperature is

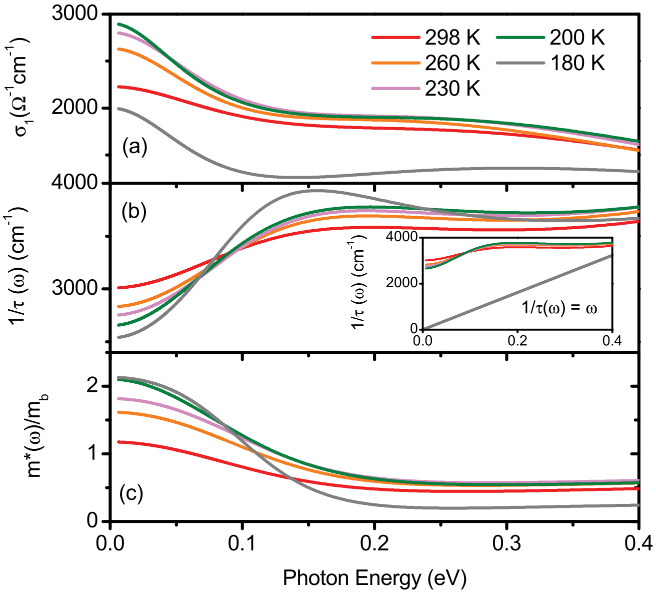

FIG. 4. (Color online) Extended Drude analysis of the metallic state of V_2O_3. Real part of the optical conductivity (a), frequency-dependent scattering rate given by Eq. (4) (b), and frequency-dependent mass enhancement factor obtained from Eq. (5) (c). The inset in panel (b) shows $1/\tau(\omega)$ plotted with the y-axis scale starting at 0 and the gray line represents $1/\tau(\omega) = \omega$.

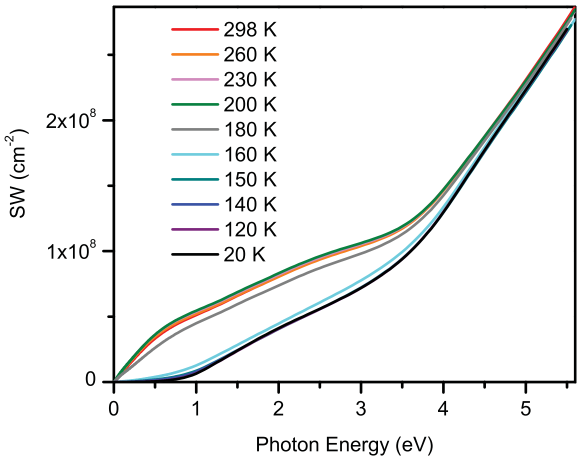

FIG. 5. (Color online) Effective electronic spectral weight of V_2O_3 obtained from the spectra in Fig. 1 using Eq. (2).

lowered toward the insulting phase, as expected in the presence of strong correlations.

We note that the analysis discussed above is based on the extended Drude model, which is intended to describe systems with a single conducting channel. V_2O_3, on the other hand, presents a two-channel conductivity. The theoretical work in Ref. 30 has shown that the contribution of the second conducting channel, characterized by the energy gap, becomes appreciable at energies of the order of the nearest-neighbor hopping (~1 eV). The extended Drude analysis presented in Fig. 4 is confined to 0.4 eV. In this range, the metallic response of V_2O_3 should, in theory, be predominantly of single-channel character.

C. Insulator-to-metal transition

As discussed above, the optical conductivity in Fig. 1 clearly shows the insulator-to-metal transition in V_2O_3 occurring around 180 K. In this section we examine the aspects of this transition in more detail, particularly as they relate to the strongly correlated nature of V_2O_3. First, we note that the insulating gap present in the optical conductivity gradually becomes filled with states as the temperature increases, without reducing the magnitude of the energy gap. This effect gives rise to a well-defined Drude mode A and an incoherent peak B and constitutes a signature of Mott-driven IMT. At the same time, the SW of the interband transitions immediately above the gap and up to 5 eV is reduced significantly. The SW(ω) at all the measured temperatures shown in Fig. 5 reveals that the optical conductivity of to 5 eV must be considered in order to fully account for the low-frequency increase in spectral weight observed across the IMT. Such a large energy scale for SW transfer is consistent with the Mott-Hubbard model: The emerging Drude response is the result of a quasiparticle peak forming at the Fermi level at the expense of the Hubbard bands, separated by an energy U.

We note that the data in Fig. 5 are at odds with earlier measurements of V_2O_3 films for which the low-temperature SW does not recover the values measured for the metallic phase even at 6 eV. This is related to the higher optical conductivity observed in the present study for the interband transitions between 1 and 3 eV. In Table I we compare the spectral weight obtained from Fig. 5 and from Ref. 19 with different energy cutoffs. From the data in Ref. 19 we find that the SW obtained for the insulating state up to 3.2 eV, where the $\sigma_1(\omega)$ curves cross, is 53% of the metallic phase SW. A similar analysis of our data yields 82%. Knowing that the bandwidth of the t_{2g} manifold in V_2O_3 is very sensitive to extrinsic factors such as doping and pressure and quite possibly strain and impurities, it is likely that this difference is associated with the higher quality of our films, evidenced also by the stronger Drude peak.

In addition to the large energy scale for SW transfer, indications of a pseudogap and the low-temperature increase in the mass enhancement factor (Fig. 4) highlight the importance of electronic correlations in driving the IMT. While evidence of a pseudogap in the optical conductivity of V_2O_3 above 450 K (in the crossover region) is presented in Ref. 24, here we focus on lower temperatures closer to the AFI to PM transition. We find that the partial gapping of the Fermi surface is occurring in spite of the high metallicity of our films, which differs from the bad-metallic behavior of the crossover phase reported in Ref. 24. Furthermore, the peak feature in $1/\tau(\omega)$ centered at 0.18 eV is more pronounced at lower temperatures, closer to the IMT. Thus, we propose that the pseudogap is linked to the AFI to PM transition and is indicative of the importance of Mott physics in this part of the V_2O_3 phase diagram.

D. Comparison to VO_2

We now compare our results to previous optical studies of the closely related correlated oxide VO_2. Starting at the far-IR part of the spectra in Fig. 1 we note that the Drude peak is

TABLE I. Comparison of spectral weight values from the present work and from Ref. 19. SW up to 1, 3.2, and 5.5 eV and the ratio of the SW in the insulating and metallic states at these energies.

	20 K[a]	200 K[a]	SW(20 K)/SW(200 K)[a]	100 K[b]	200 K[b]	SW(20 K)/SW(200 K)[b]
SW(1 eV) (cm^{-1})	6.46×10^6	5.45×10^7	0.12	2.06×10^6	2.24×10^7	0.09
SW(3.2 eV) (cm^{-1})	8.02×10^7	9.75×10^7	0.82	3.58×10^7	6.70×10^7	0.53
SW(5.5 eV) (cm^{-1})	2.66×10^8	2.75×10^8	0.97	1.48×10^8	1.68×10^8	0.88

[a] Present work.

[b] Reference 19.

much narrower than that observed in VO_2, which extends up to a minimum in $\sigma_1(\omega)$ at 1.7 eV.[19,31] The plasma frequency of VO_2 is thus more than two times higher than the $\omega_p = 1.25$ eV we have obtained for V_2O_3. From the extended Drude analysis we find that the peak structure found in $1/\tau(\omega)$ in Fig. 4(b) indicating the formation of a pseudogap as the IMT is approached is not present in VO_2.[31] Additionally, the mass enhancement factor is higher in V_2O_3. All these observations indicated that electronic correlations are stronger in V_2O_3 than in VO_2.

On the other hand, the optical conductivity of the metallic puddles found in the phase coexistence regime across the IMT in VO_2 bear a closer resemblance to our data.[21] In this case, the $\sigma_1(\omega)$ spectra in Fig. 4 of Ref. 21 exhibit a very narrow Drude mode followed by a dip and an incoherent peak centered at 0.25 eV, similar to the V_2O_3 data in Fig. 4(a). Furthermore, the scattering rate reveals evidence of a pseudogap, albeit much more marked than in our V_2O_3 data. We propose that this similarity between the V_2O_3 data and that of the more strongly correlated metallic puddles of VO_2 could signify a difference in the way the IMT takes place in these two vanadates. In VO_2, the strongly correlated metallic regions form within an insulating background and grow as the temperature is increased, eventually taking over the entire sample and transitioning into the rutile metal phase. In order to observe the large mass enhancement and the pseudogap it was necessary to separate the contributions from the metallic and insulating regions across the transition. In V_2O_3, on the other hand, the IMT could be occurring in a much more homogenous manner with less spatial variation of the optical constants on the nanoscale. Evidence of the very strongly correlated nature of the V_2O_3 metal near the transition can thus be observed even in far-field measurements averaging over the optical constants of macroscopic regions.

A similar contrast is evident in time-resolved spectroscopy studies of the photoinduced phase transition in VO_2 (Ref. 32) and V_2O_3.[33] In the former, the fluence required to drive the system across the IMT decreases as the temperature approaches T_c. The authors of Ref. 32 attribute this phenomenon to the percolative nature of the transition: The presence of metallic precursors reduces the amount of energy needed to reach the homogeneous metallic state. This dependence of the threshold fluence on the initial temperature of the sample is not reported for V_2O_3,[33] consistent with our proposal that phase separation in the vicinity of the IMT is more prominent in VO_2. In addition to the far-field and time-domain spectroscopy studies of V_2O_3, low-temperature scanning near-field infrared microscopy would be the ideal tool to further investigate this issue.

Finally, we comment on an important difference between the phase diagrams of the two materials. While VO_2 exhibits a single IMT at 340 K, V_2O_3 presents a high-temperature crossover phase with poor metallic properties,[17] in addition to the paramagnetic metallic and antiferromagnetic insulating phases studied here. By applying external pressure or doping with chromium, the temperature range over which the sample is metallic is significantly reduced and a high-temperature paramagnetic insulating phase emerges.[14,18] Thus, as the temperature is raised beyond $T_c \approx 150$ K, V_2O_3 enters the metallic state but then begins to approach the crossover region, precluding the system from evolving into a less correlated metal like VO_2 does. For this reason, the spectra in Figs. 1 and 4 have more in common with the metallic puddles found very close to the IMT in VO_2 (Ref. 21) than with the high-temperature rutile phase away from the transition.[31] Furthermore, $K_{\mathrm{exp}}/K_{\mathrm{LDA}} \approx 0.5$ for VO_2,[19,27] much higher than the value we have obtained for V_2O_3. This interpretation is consistent with studies of chromium-doped V_2O_3,[18] where the optical conductivity of the paramagnetic metallic phase exhibits a bad metal behavior with no well-defined Drude peak,[34] suggestive of enhanced correlations in the region between the antiferromagnetic and paramagnetic insulating states.

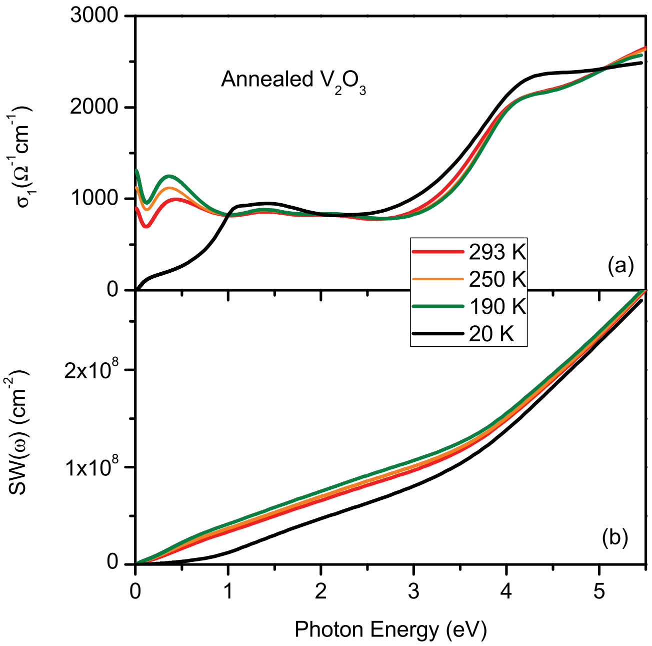

FIG. 6. (Color online) Real part of the optical conductivity (a) and effective spectral weight (b) obtained for the annealed V_2O_3 sample.

E. Annealed V_2O_3

In Fig. 6(a) we show the optical conductivity obtained for the annealed V_2O_3 film. It is immediately evident that the magnitudes of the Drude mode and the incoherent peak B are dramatically suppressed compared to the data for the pristine sample (Fig. 1). Additionally, the difference between the spectral weight of the interband transitions up to 5 eV in the insulating and metallic states is not as marked as it is in Fig. 1. SW(ω) at 5.5 eV however, is similar for both samples [Figs. 5 and 6(b)]. In other words, the annealing process causes a redistribution of SW in the metallic state, from the low-frequency features associated with the e_g^π and a_{1g} QP to the optical conductivity above 1 eV related to the Hubbard bands. Finally, we note that the weak Drude and the incoherent peak of comparable magnitude are reminiscent of earlier data for V_2O_3 thin films,[19] although the dc conductivity reported here is still a factor of 2 higher than in Ref. 19. We thus conclude that the enhanced Drude spectral weight we have measured in our pristine V_2O_3 films is indeed related to an increased QP density of states and cannot be attributed solely to an overall shift in the $\sigma_1(\omega)$ values.

IV. CONCLUSIONS

We have presented an optical study of V_2O_3 thin films providing interesting information about the metallic state and the AFI to PM transition in this material. We find that the temperature-driven transfer of spectral weight, both within the metallic state and across the IMT, is consistent with the Mott-Hubbard model for correlated systems. The extended Drude analysis, facilitated by the well-defined coherent response of our sample, reveals signatures of strong correlations in the metallic state: (i) the formation of a pseudogap as a possible interpretation of our data and (ii) the enhancement of the carrier effective mass as the IMT is approached. Finally, we propose that the similarities between our data and the metallic puddles of phase separated VO_2 indicate that electronic correlations remain quite prevalent even as temperatures are raised past the immediate vicinity of the IMT.

ACKNOWLEDGMENTS

Work at UCSD was funded by DOE and AFOSR-MURI.

---

[*] mstewart@physics.ucsd.edu

[1] M. Imada, A. Fujimori, and Y. Tokura, Rev. Mod. Phys. **70**, 1039 (1998).

[2] D. N. Basov, R. D. Averitt, D. van der Marel, M. Dressel, and K. Haule, Rev. Mod. Phys. **85**, 471 (2011).

[3] P. D. Dernier and M. Marezio, Phys. Rev. B **2**, 3771 (1970).

[4] M. J. Rozenberg, G. Kotliar, H. Kajueter, G. A. Thomas, D. H. Rapkine, J. M. Honig, and P. Metcalf, Phys. Rev. Lett. **75**, 105 (1995).

[5] M. J. Rozenberg, G. Kotliar, and H. Kajueter, Phys. Rev. B **54**, 8452 (1996).

[6] J. H. Park, L. H. Tjeng, A. Tanaka, J. W. Allen, C. T. Chen, P. Metcalf, J. M. Honig, F. M. F. de Groot, and G. A. Sawatzky, Phys. Rev. B **61**, 11506 (2000).

[7] K. Held, G. Keller, V. Eyert, D. Vollhardt, and V. I. Anisimov, Phys. Rev. Lett. **86**, 5345 (2001).

[8] F. Mila, R. Shiina, F.-C. Zhang, A. Joshi, M. Ma, V. Anisimov, and T. M. Rice, Phys. Rev. Lett. **85**, 1714 (2000).

[9] L. Paolasini, C. Vettier, F. de Bergevin, F. Yakhou, D. Mannix, A. Stunault, W. Neubeck, M. Altarelli, M. Fabrizio, P. A. Metcalf, and J. M. Honig, Phys. Rev. Lett. **82**, 4719 (1999).

[10] S. Di Matteo, N. B. Perkins, and C. R. Natoli, Phys. Rev. B **65**, 054413 (2002).

[11] N. B. Perkins, S. Di Matteo, and C. R. Natoli, Phys. Rev. B **80**, 165106 (2009).

[12] A. Tanaka, J. Phys. Soc. Jpn. **71**, 1091 (2002).

[13] S.-K. Mo, J. D. Denlinger, H.-D. Kim, J.-H. Park, J. W. Allen, A. Sekiyama, A. Yamasaki, K. Kadono, S. Suga, Y. Saitoh, T. Muro, P. Metcalf, G. Keller, K. Held, V. Eyert, V. I. Anisimov, and D. Vollhardt, Phys. Rev. Lett. **90**, 186403 (2003).

[14] D. B. McWhan, T. M. Rice, and J. P. Remeika, Phys. Rev. Lett. **23**, 1384 (1969).

[15] A. Jayaraman, D. B. McWhan, J. P. Remeika, and P. D. Dernier, Phys. Rev. B **2**, 3751 (1970).

[16] P. Limelette, A. Georges, D. Jerome, P. Wzietek, P. Metcalf, and J. M. Honig, Science **302**, 89 (2003).

[17] A. Perucchi, L. Baldassarre, P. Postorino, and S. Lupi, J. Phys.: Condens. Matter **21**, 323202 (2009).

[18] F. Rodolakis, P. Hansmann, J. P. Rueff, A. Toschi, M. W. Haverkort, G. Sangiovanni, A. Tanaka, T. Saha-Dasgupta, O. K. Andersen, K. Held, M. Sikora, I. Alliot, J. P. Itie, F. Baudelet, P. Wzietek, P. Metcalf, and M. Marsi, Phys. Rev. Lett. **104**, 047401 (2010).

[19] M. M. Qazilbash, A. A. Schafgans, K. S. Burch, S. J. Yun, B. G. Chae, B. J. Kim, H. T. Kim, and D. N. Basov, Phys. Rev. B **77**, 115121 (2008).

[20] M. M. Qazilbash, M. Brehm, B.-G. Chae, P. C. Ho, G. O. Andreev, B.-J. Kim, S. J. Yun, A. V. Balatsky, M. B. Maple, F. Keilmann, H.-T. Kim, and D. N. Basov, Science **318**, 1750 (2007).

[21] M. M. Qazilbash, M. Brehm, G. O. Andreev, A. Frenzel, P. C. Ho, B. G. Chae, B. J. Kim, S. J. Yun, H. T. Kim, A. V. Balatsky, O. G. Shpyrko, M. B. Maple, F. Keilmann, and D. N. Basov, Phys. Rev. B **79**, 075107 (2009).

[22] M. K. Stewart, C. H. Yee, J. Liu, M. Kareev, R. K. Smith, B. C. Chapler, M. Varela, P. J. Ryan, K. Haule, J. Chakhalian, and D. N. Basov, Phys. Rev. B **83**, 075125 (2011).

[23] M. K. Stewart, J. Liu, M. Kareev, J. Chakhalian, and D. N. Basov, Phys. Rev. Lett. **107**, 176401 (2011).

[24] L. Baldassarre, A. Perucchi, D. Nicoletti, A. Toschi, G. Sangiovanni, K. Held, M. Capone, M. Ortolani, L. Malavasi, M. Marsi, P. Metcalf, P. Postorino, and S. Lupi, Phys. Rev. B **77**, 113107 (2008).

[25] S. Y. Ezhov, V. I. Anisimov, D. I. Khomskii, and G. A. Sawatzky, Phys. Rev. Lett. **83**, 4136 (1999).

[26] A. I. Poteryaev, J. M. Tomczak, S. Biermann, A. Georges, A. I. Lichtenstein, A. N. Rubtsov, T. Saha-Dasgupta, and O. K. Andersen, Phys. Rev. B **76**, 085127 (2007).

[27] M. M. Qazilbash, J. J. Hamlin, R. E. Baumbach, L. J. Zhang, D. J. Singh, M. B. Maple, and D. N. Basov, Nat. Phys. **5**, 647 (2009).

[28] M. K. Stewart, J. Liu, R. K. Smith, B. C. Chapler, C. H. Yee, D. Meyers, R. E. Baumbach, M. B. Maple, K. Haule, J. Chakhalian, and D. N. Basov, J. Appl. Phys. **110**, 033514 (2011).

[29] D. N. Basov and A. V. Chubukov, Nat. Phys. **7**, 272 (2011).

[30] Y. Song and L.-J. Zou, Eur. Phys. J. B **72**, 59, (2009).

[31] M. M. Qazilbash, K. S. Burch, D. Whisler, D. Shrekenhamer, B. G. Chae, H. T. Kim, and D. N. Basov, Phys. Rev. B **74**, 205118 (2006).

[32] D. J. Hilton, R. P. Prasankumar, S. Fourmaux, A. Cavalleri, D. Brassard, M. A. El Khakani, J. C. Kieffer, A. J. Taylor, and R. D. Averitt, Phys. Rev. Lett. **99**, 226401 (2007).

[33] M. K. Liu, B. Pardo, J. Zhang, M. M. Qazilbash, S. J. Yun, Z. Fei, J. H. Shin, H. T. Kim, D. N. Basov, and R. D. Averitt, Phys. Rev. Lett. **107**, 066403 (2011).

[34] S. Lupi, L. Baldassarre, B. Mansart, A. Perucchi, A. Barinov, P. Dudin, E. Papalazarou, F. Rodolakis, J. P. Rueff, J. P. Itie, S. Ravy, D. Nicoletti, P. Postorino, P. Hansmann, N. Parragh, A. Toschi, T. Saha-Dasgupta, O. K. Andersen, G. Sangiovanni, K. Held, and M. Marsi, Nat. Comm. **1**, 105 (2010).